

KRISHNAN, R.R., KAVITHA, V.S., CHALANA, S.R., PRABHU, R. and PILLAI, V.P.M. 2019. Effect of tungsten doping on the properties of In_2O_3 films. JOM: journal of the minerals, metals and materials society [online], 71(5), pages 1885-1896.

Available from: <https://doi.org/10.1007/s11837-019-03426-7>

Effect of tungsten doping on the properties of In_2O_3 films.

KRISHNAN, R.R., KAVITHA, V.S., CHALANA, S.R., PRABHU, R. and PILLAI, V.P.M.

2019

This is a post-peer-review, pre-copyedit version of an article published in JOM Journal of the Minerals, Metals and Materials Society. The final authenticated version is available online at:

<http://dx.doi.org/10.1007/s11837-019-03426-7>

OpenAIR
@RGU

This document was downloaded from
<https://openair.rgu.ac.uk>



Effect of tungsten doping on the properties of In₂O₃ films

Reshmi Krishnan R¹, Kavitha V. S¹, Chalana S. R¹, Radhakrishna Prabhu² and V. P. Mahadevan Pillai^{1*}

¹Department of Optoelectronics, University of Kerala, Thiruvananthapuram, Kerala, India.

²School of Engineering, Robert Gordon University, Aberdeen, UK

*Corresponding author. Tel.: +91 471 2412167, email- vpmpillai9@gmail.com

ABSTRACT

Highly crystalline tungsten doped indium oxide (In₂O₃) films are synthesized at room temperature by RF magnetron sputtering technique. The structural and morphological properties of the as-deposited films and the films annealed at a temperature of 300°C are investigated in detail. XRD analysis reveals the presence of cubic bixbyite structure with preferred orientation along (222) plane for both the as-deposited and annealed films. Moderate tungsten doping (1 wt%) enhances the crystallinity of the as-deposited In₂O₃ films whereas the crystallinity of the films systematically decreases with increase in tungsten doping concentration beyond 1 wt%. Raman spectral analysis discloses the modes of cubic bixbyite In₂O₃ phase in the films. AFM micrographs show a smooth and dense distribution of smaller grains in the films. XPS reveals the existence of W⁵⁺ in the doped films. The undoped film is highly oxygen deficient. Variation in the concentration of oxygen vacancy can be associated with the degree of crystallinity of the films.

Keywords: effect of tungsten doping, nanostructured indium oxide films, structural properties, XPS analysis

Introduction

Metal oxide materials in the nanoscale have emerged as vital components in micro/nanoscale devices due to their astounding physical and chemical properties which are dependent on their shape, size/dimensionality, morphology, crystallographic orientation, high transmittance/reflective properties, high conductivity, wide band gap, etc. [1-3]. Among these, indium oxide (In₂O₃) and indium oxide based thin films have great technological applications owing to their various fascinating aspects including high visible transparency, good electrical conductivity, long-term stability and higher catalytic properties [4-6]. Apart from their widespread applications in electrooptic modulators, low-emissivity windows, solar cells, flat-panel displays, gas sensors, electrochromic mirrors etc. [7-9], impurity added In₂O₃ is found to be suitable as dilute magnetic semiconductors for spintronic applications [10,11]. In₂O₃ can exist in two different crystal structures namely cubic bixbyite structure and

rhombohedral structure [12]. In_2O_3 films prepared using different deposition methods may be single crystalline-like or polycrystalline but they mostly possess the cubic bixbyite structure independent of the substrate used [13]. The cubic bixbyite In_2O_3 structure is thermodynamically stable while the rhombohedral phase is the metastable phase [14,15]. The formation of rh- In_2O_3 requires high temperature and pressure conditions [12]. Intrinsic defects (oxygen vacancies, interstitials etc.) in the undoped film can alter its properties. Doping with suitable dopant material is one of the ways to improve its properties [16]. Tungsten with a lower ionic radius and higher oxidation state compared to In^{3+} cation can be a good dopant for In_2O_3 lattice. It is reported that tungsten doped indium oxide films have high mobility, low electrical resistivity and high transparency in the visible and near infrared region [17-22]. Structural properties can affect the quality of thin films thereby modifying their optical, electrical, sensing properties etc. Thus, these characteristics play a prime role in the technological point of view as these are needed to fabricate films with desired properties [23]. To the best of our knowledge, there are no reports on the effect of tungsten doping concentration on the structural properties of RF sputtered In_2O_3 films prepared at room temperature in argon (Ar) ambience. Yan et al., reported the effect of RF power on tungsten and titanium doped In_2O_3 films fabricated using RF magnetron sputtering at room temperature [24]. They also studied the changes in the structural and electrical characteristics of the vacuum post annealed films. By reactive plasma deposition, Lu et al., [25] synthesized W-doped In_2O_3 films at room temperature for different O_2/Ar ratios. The influence of annealing temperature on the structural, electrical and optical properties was also investigated [25]. Pan et al., reported the role of sputtering power and thickness on the structural, morphological and optoelectrical properties of W-doped In_2O_3 films at room temperature using reactive magnetron sputtering [20]. Samatov et al. [22] investigated the effect of tungsten doping percentage and fraction of O_2 dilution in the sputtering gas on the optoelectrical and structural properties of RF sputtered In_2O_3 films. Free electron concentration generated by the dopant tungsten and due to oxygen vacancies was also studied. Amorphous W-doped In_2O_3 films exhibiting smooth surface morphology were reported.

This paper reports an in-depth analysis of the role of tungsten doping on the structural and morphological properties of highly crystalline RF sputtered In_2O_3 films at room temperature. Also, the effect of annealing at a temperature of 300 °C on the properties of In_2O_3 films is investigated. Structural and morphological analyses were performed using techniques such as X-ray diffraction (XRD), micro-Raman spectroscopy, X-ray photoelectron spectroscopy (XPS) and atomic force microscopy (AFM).

Experiment

Tungsten doped In_2O_3 films were fabricated by sputtering technique (RF magnetron). In_2O_3 powder (99.99% purity) was mixed with WO_3 powder (99.99% purity) in desired proportions namely 0, 1, 2, 3 and 4 wt%) and the well-grounded mixtures were used as sputtering targets. The deposition was carried out in a chamber evacuated to a base pressure of 4×10^{-6} mbar and under an argon pressure of 0.015 mbar for 40 minutes with an RF power of 120 W (magnetron power supply - Advanced Energy, MDX 500). The films were deposited on quartz substrates kept at distance of 5 cm from the target. The as-deposited films with tungsten doping concentrations (viz., 0, 1, 2, 3 and 4 wt%) are coded as IW0, IW1, IW2, IW3 and IW4 respectively and the films annealed in air at a temperature of 300°C are coded as IW0(300), IW1(300), IW2(300), IW3(300) and IW4(300) respectively. Both the as-deposited and annealed films are used for characterization.

The structure of the films was studied by X-ray diffractometer (Bruker AXS D8 Advance) using X-ray wavelength 1.5406 Å (Cu $K\alpha_1$ radiation). The measurements were done in the 2θ range 20° - 70° using Bragg-Brentano geometry at a scan rate of 0.02° per minute. Raman spectra of the film samples were obtained using Labram HR-800 micro-Raman spectrometer (Horiba Jobin Yvon). An excitation radiation of 514.5 nm from argon ion laser was employed to record the spectra. Bruker-Dimension Edge atomic force microscope (Si tip on nitride lever having force constant 0.4 N/m) in ScanAsyst mode was used for surface profiling of the films. The oxidation states of the elements are estimated by X-ray photoelectron (XPS) spectrometer (Omicron Technology) with monochromatic $\text{AlK}\alpha$ (1486.7 eV) X ray source. CASA XPS software was used for the XPS data analysis.

Results and discussion

Fig. 1 shows the XRD patterns of the as-deposited tungsten doped In_2O_3 thin films with different levels of tungsten doping. As evidenced by the presence of intense peaks, XRD patterns suggest a polycrystalline nature for all the films. Earlier reports show that In_2O_3 films crystallize only at a temperature of $\sim 150^\circ\text{C}$ [26]. The deposition temperature is monitored using a thermo-couple and it shows that the temperature in the chamber during deposition was between 40-50 °C. It is interesting to note that in the present study, the as-deposited films, though they are deposited on unheated quartz substrate, possess good crystalline quality. In sputtering systems, the sputtered particles may have high value of kinetic energy (\sim several eV) and this may increase the surface migration of the particles to reach the substrate effectively to produce crystalline films [27]. Park et al. [28]

reported that continuous energetic ion bombardment can be the source of crystallization of films on unheated substrates.

The XRD pattern of the IW0 film presents an intense peak at $2\theta = 30.66^\circ$, a medium intense peak at 51.12° and five weak peaks at 2θ values 21.55° , 41.95° , 45.76° , 59.09° and 60.14° . These peaks belong to the cubic bixbyite structure of In_2O_3 and they can be indexed to lattice reflection planes (222), (440), (211), (332), (431), (541) and (622) respectively [JCPDS file No. 71-2195]. The presence of the hump like structure in the 2θ range $20\text{-}30^\circ$ and the less intensity of the XRD peaks indicate the less-crystalline nature of the undoped film. Tungsten doping in In_2O_3 lattice seems to have profound effect on its crystallinity which is quite evident from the intensity modification in the XRD patterns. The XRD intensity exhibited by the doped films are much higher than that of the undoped film. In all the as-deposited films, (222) peak shows the highest intensity indicating that $\langle 111 \rangle$ is the preferred direction of growth of crystallites in them.

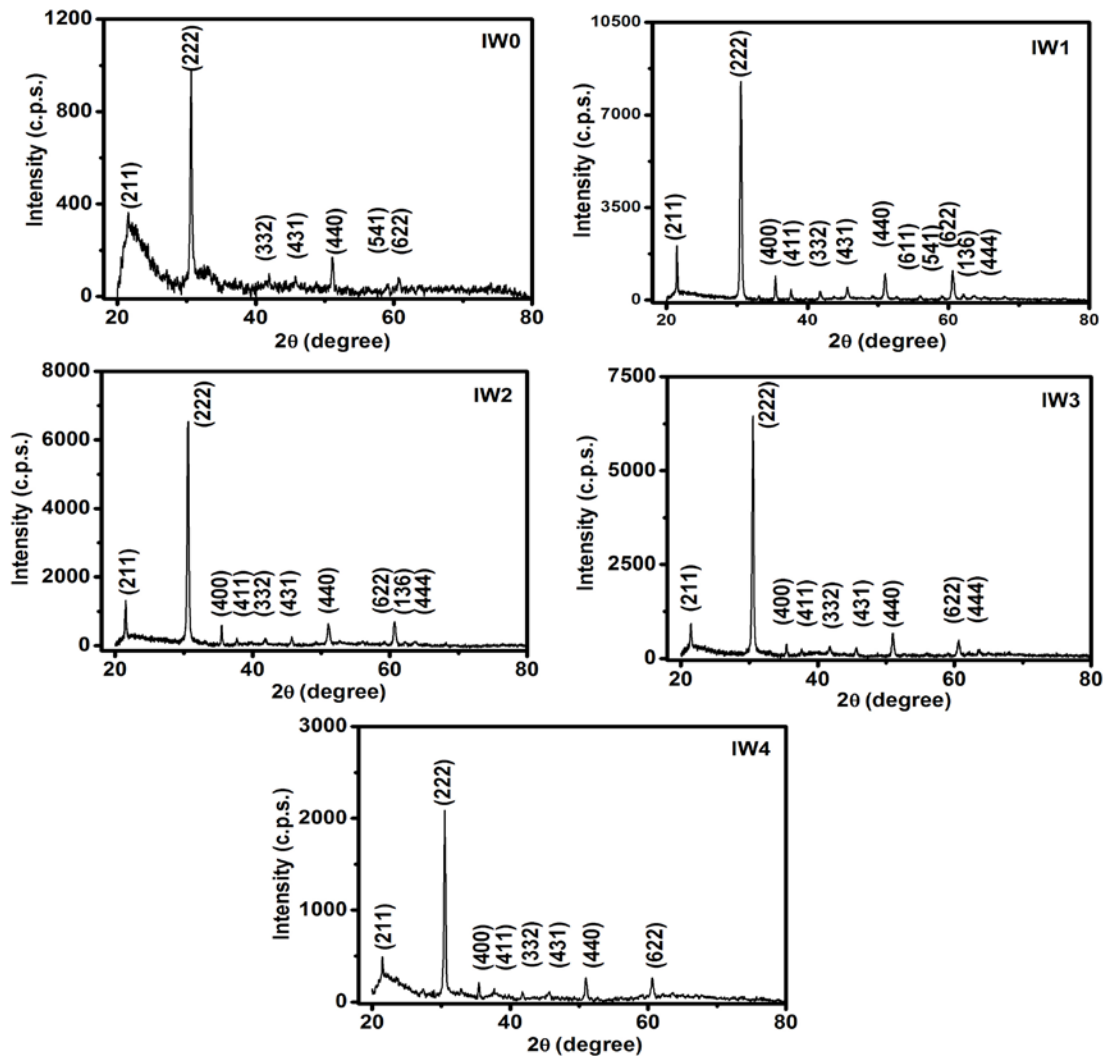


Fig. 1. XRD patterns of as-deposited tungsten doped In_2O_3 films deposited on quartz substrate by RF magnetron sputtering technique.

A moderate doping of tungsten (i.e. 1 wt%) enhances the crystalline quality of the film drastically as evidenced by the very high intensity in the XRD pattern. Further increase in the tungsten doping results in a systematic decrease in the intensity of (222) peak (Fig. 3(a)). The intensities of the (222) peak in IW1, IW2, IW3 and IW4 are respectively 8.70, 6.86, 6.69 and 2.13 times that of IW0 film. This indicates that tungsten doping in In_2O_3 lattice improves its crystallinity even under as-deposited condition and the crystallinity of the IW1 film is superior compared to other films. Hence, the optimum value of tungsten doping to get high quality crystalline films in the as-deposited condition is 1 wt%.

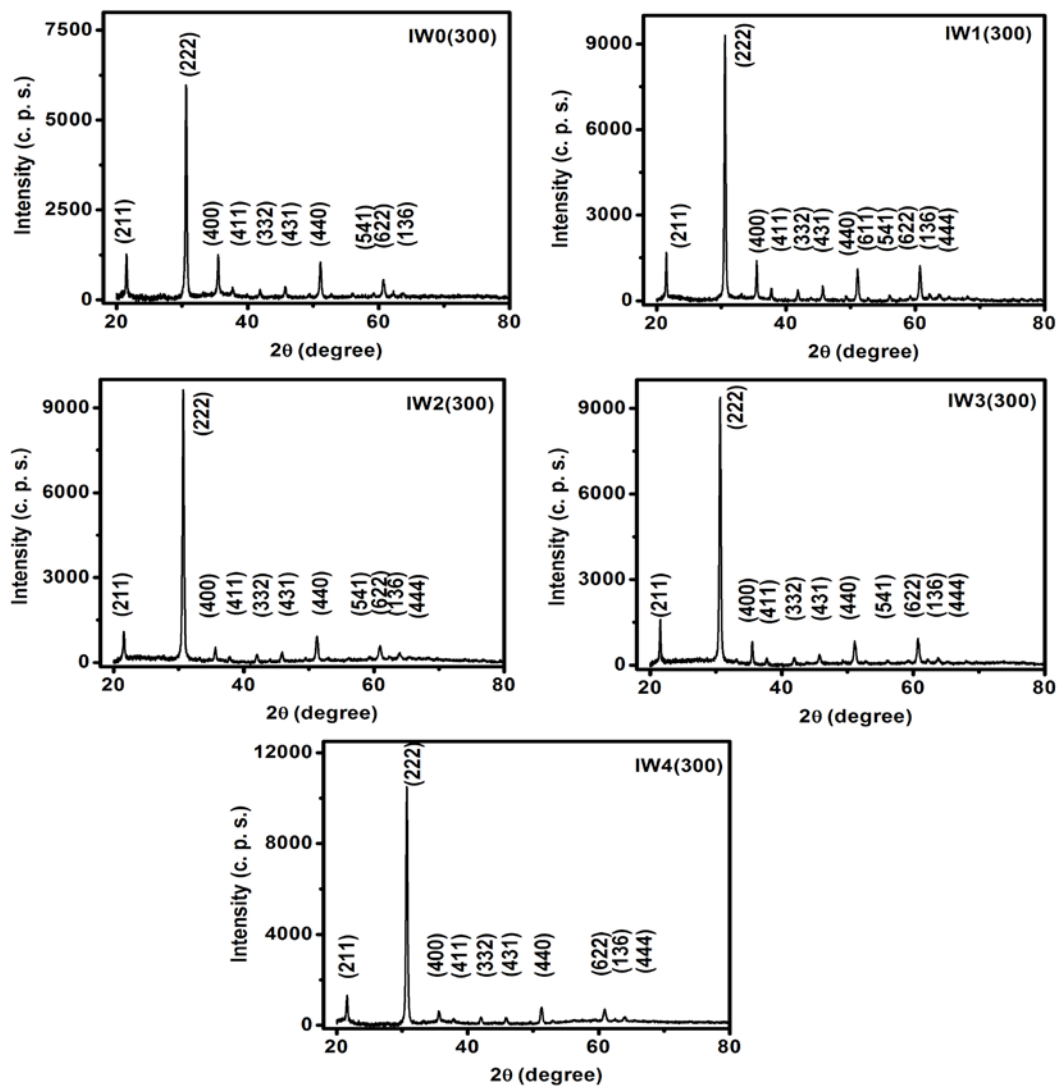


Fig. 2. XRD patterns of tungsten doped In_2O_3 films annealed at a temperature of 300 °C.

Fig. 2 represents the XRD patterns of the tungsten doped films annealed at a temperature 300 °C. All the peaks in the XRD pattern of the annealed films can be indexed to the cubic bixbyite phase of In_2O_3 . Also, in the annealed films $\langle 111 \rangle$ is the preferred direction of crystalline growth. Annealing of the films in air for 1 hour at a temperature 300 °C enhances the intensity of the most intense peak (222) compared to that in the as-deposited counter parts (Fig. 3(a)). Some additional peaks are also observed in the XRD patterns of all the annealed films. The enhancement in the XRD peak intensities as well as the appearance of additional peaks in the annealed films indicates an improvement in the crystallinity compared to the as-deposited films.

Among the as-deposited films, the IW0 film shows the least value of XRD intensity. On annealing, its intensity enhanced by 6.25 times compared to that of as-deposited film. In the as-deposited film, there may be defects due to oxygen vacancy and other lattice disorders. On thermal annealing, oxygen vacancies get filled, lattice disorders decrease, stoichiometry improves and hence crystallinity increases. Compared to In_2O_3 , WO_3 is an oxygen rich entity. Doping of In_2O_3 with WO_3 can provide more oxygen to the lattice and oxygen vacancies get filled and the film becomes more stoichiometric. This can be the reason for the improvement in crystallinity of the tungsten doped In_2O_3 films in the as-deposited conditions. But when the doping level increases beyond an optimum level, stress and defects in the film can increase and hence, the highest doped film IW4 shows the lowest XRD intensity among the doped as-deposited films. On thermal annealing, the stress gets released and defects may get reduced. Among the annealed films, IW4(300) film shows the highest intensity. The intensity of the (222) peak in IW4(300) film is about 5.09 times that of the IW4 film.

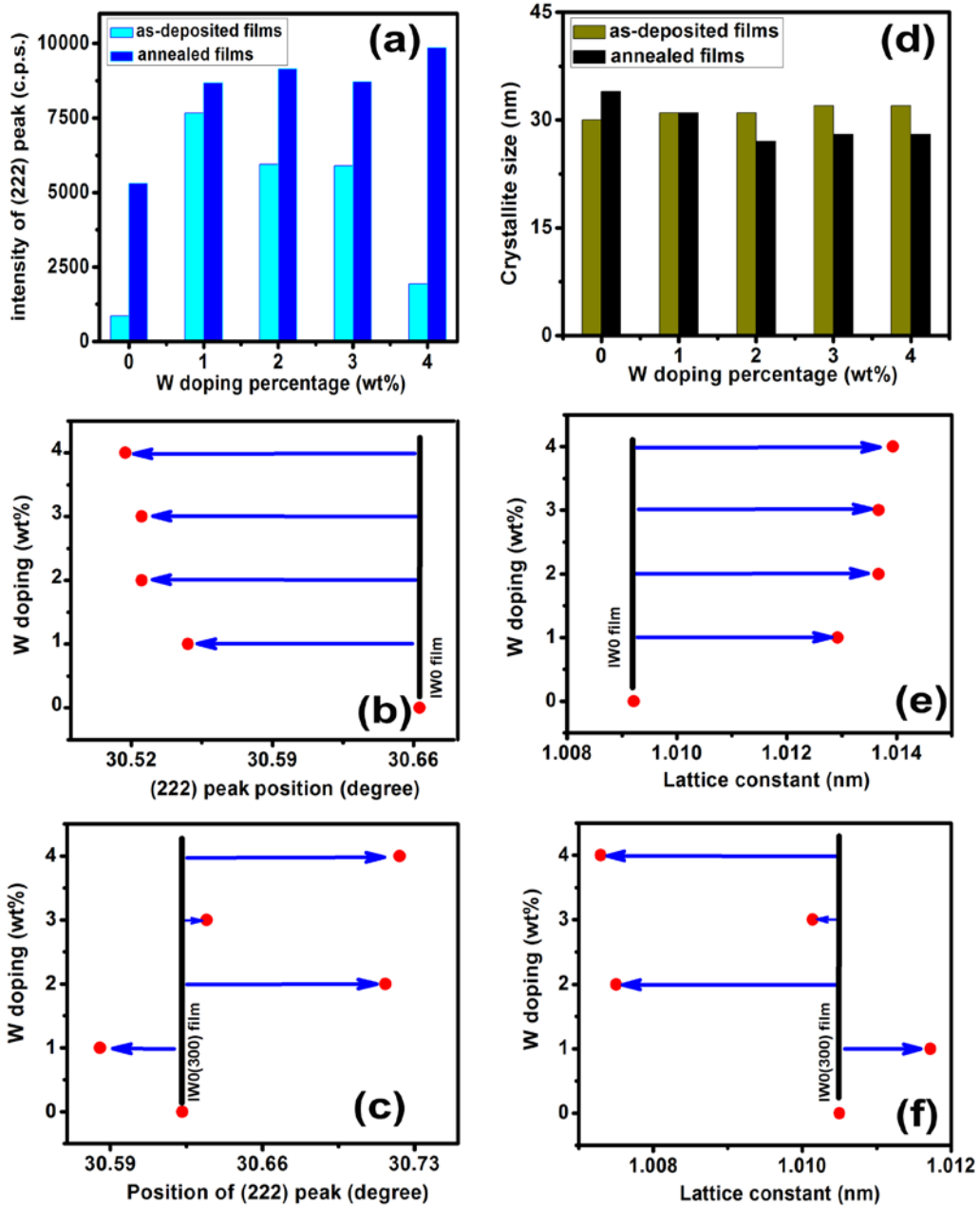


Fig. 3. (a) Variation of intensity of (222) peak in the as-deposited and annealed films with tungsten doping concentration, (b), (c) variation of position of (222) peak with tungsten doping concentration for as-deposited and annealed films respectively, (d) variation of crystallite size in the as-deposited and annealed films with tungsten doping concentration and (e), (f) variation of lattice constant with tungsten doping concentration in the as-deposited and annealed films respectively.

In the IWO film, the (222) peak is observed at a 2θ value 30.66° . In the doped as-deposited films, this peak shifts to lower 2θ values (Fig. 3(b)). In the IWO(300) film, the (222) peak is observed at a 2θ value 30.623° .

In the IW0(300) film, this peak shifts to lower 2θ values while in other doped annealed films, this peak shifts to higher 2θ values (Fig. 3(c)).

The lattice constant 'a' for a cubic system is calculated from the interplanar spacing d of the intense (222) peak by the following relation [29]:

$$\frac{1}{d^2} = \frac{h^2 + k^2 + l^2}{a^2} \quad (1)$$

where h, k and l are the Miller indices. The calculated values of lattice constant for the as-deposited and annealed films are shown in Fig 3(e) and 3(f) respectively and in Table 1. In the as-deposited films, the value of lattice constant increases due to tungsten doping compared to undoped film IW0. But in the annealed doped films, the value of lattice constant decreases except for IW1(300) film compared to the IW0 film. In the IW1(300) film, lattice constant shows a slight increase compared to the film IW0. The ionic radii of the different tungsten ions are: W^{4+} -0.066 nm [25], W^{5+} -0.062 [30], W^{6+} -0.060 nm [25]. For all these tungsten ions, the ionic radii are less compared to that of In ions (In^{3+} -0.081 nm) [31]. The crystal lattice contracts and lattice constant decreases when dopant ions of smaller radii are substituted for host ions of larger radii [32]. But in the as-deposited films, the observed values of lattice constant are not in line with this argument. The enhancement of the lattice constant suggests an expansion of the lattice. Meng et al. [33] observed higher values of lattice constant for Mo doped In_2O_3 films though the ionic radius of Mo^{6+} (0.062 nm) is smaller than that of In^{3+} ions (0.081 nm) [33]. Shukla et al. [34] also observed an expansion of lattice when ZnO is doped with Al^{3+} ions of lower ionic radii (0.53 Å) compared to that of Zn^{2+} ions (0.72 Å) for higher doping levels. They attributed this to the possibility of having Al^{3+} ions in the interstitial position. The lattice mismatch, strain effects and mismatch between the ions, impurities and defects can also lead to expansion of lattice [35-37]. Since the films are as-deposited, the dopant ions may not have sufficient energy to diffuse into the appropriate In^{3+} sites. But in the annealed films except for the IW1(300) film, the lattice constant shows lower values suggesting a contraction of lattice and substitution of In^{3+} sites by tungsten ions. On annealing, tungsten ions may get sufficient energy to diffuse into the appropriate In^{3+} sites and gets substituted. Also, thermal annealing reduces the defects and strain effects in the film. The value of the lattice constant observed for IW1(300) film is 1.0117 nm almost identical to the bulk In_2O_3 [1.0118 nm-JCPDS file No. 71-2195]. All the doped films annealed at 300°C show a lower value of lattice constant compared to their as-deposited analogues.

The mean value of the size of the crystallites D_{hkl} can be calculated by employing the following Scherrer equation using the peak position ($2\theta_{hkl}$) and the full width at half maximum in radians (β_{hkl}) [38]:

$$D_{hkl} = \frac{0.9\lambda}{\beta_{hkl} \cos \theta_{hkl}} \quad (2)$$

Here λ is the X-ray wavelength. The calculated values of crystallite size in the as-deposited and annealed films are listed in Table 1 and the observed size suggests the nanostructured nature of the films. The effect of tungsten doping and thermal annealing on the mean size of the crystallites is illustrated in Fig 3(d).

The reduction in the size of the crystallites and strain in the films can broaden the XRD peaks. The strain free crystallite size (D'_{hkl}) can be determined by using Williamson-Hall (W-H) plot analysis by the following relation [39]:

$$\beta_{hkl} \cos \theta_{hkl} = \frac{k\lambda}{D'_{hkl}} + 2\eta \sin \theta_{hkl} \quad (3)$$

where θ_{hkl} is the half of the diffraction angle, k is the correction shape factor which can be taken as 0.9 for spherical grains and η is the residual strain. W-H plots for the as-deposited and annealed tungsten doped In_2O_3 films are shown in Fig. 3(g) and Fig. 3(h). The crystallite size and strain in the films are estimated from the linear fit of $\beta \cos \theta$ versus $\sin \theta$. The size of the crystallites and strain can be evaluated from the y-intercept and slope respectively. The dissimilarity in the crystallite size estimated using the Scherrer formula and WH-plot (Table I) manifests the presence of strain induced peak broadening in the films.

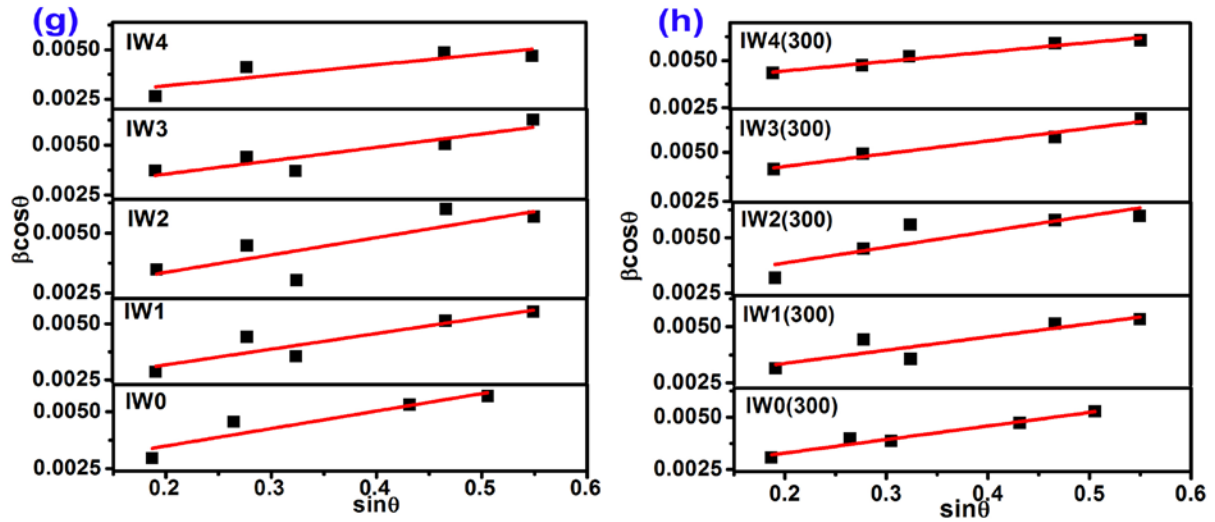


Fig. 3. Williamson-Hall (W-H) plot of tungsten doped In₂O₃ films: (g) as-deposited (h) annealed at a temperature of 300 °C.

Table I Structural parameters of as-deposited and annealed tungsten doped In₂O₃ films on quartz substrate by RF magnetron sputtering.

W doping level (wt %)	Lattice constant (nm)		Crystallite size (nm)				Lattice strain from W-H plot	
	As-deposited films	Annealed films	As-deposited films		Annealed films		As-deposited films	Annealed films
			From Scherrer formula	From W-H plot	From Scherrer formula	From W-H plot		
0	1.0092 ±0.0255	1.0105 ±0.0241	30 ±1.15	71 ±27	34 ±1.44	70 ±13	0.0037 ±0.0010	0.0032 ±0.0377
1	1.0129 ±0.0219	1.0117 ±0.0229	31 ±1.49	85 ±30	31 ±1.49	67 ±25	0.0039 ±0.0010	0.0033 ±0.0009
2	1.0137 ±0.0212	1.0075 ±0.0276	31 ±1.56	77 ±40	27 ±0.93	61 ±28	0.0041 ±0.0017	0.0040 ±0.0012
3	1.0137 ±0.0212	1.0101 ±0.0245	32 ±1.61	67 ±17	28 ±1.13	49 ±06	0.0038 ±0.0010	0.0037 ±0.0452
4	1.0139 ±0.0210	1.0073 ±0.0279	32 ±1.63	70 ±22	28 ±0.95	42 ±02	0.0030 ±0.0012	0.0028 ±0.0294

The vibrational analyses of the as-deposited and annealed tungsten doped In₂O₃ films are done using micro-Raman spectroscopy. The micro-Raman spectra of tungsten doped In₂O₃ films without annealing are

shown in Fig. 4(a). Two very low frequency sets at 103 and 130 cm^{-1} , two low frequency sets at 302 and 366 cm^{-1} , and two high frequency sets at 494 and 629 cm^{-1} are reported as the vibrational modes for cubic bixbyite In_2O_3 phase by Gan et al. [40]. The presence of these modes in the Raman spectra of all the films supports the formation of cubic bixbyite In_2O_3 crystalline phase [41].

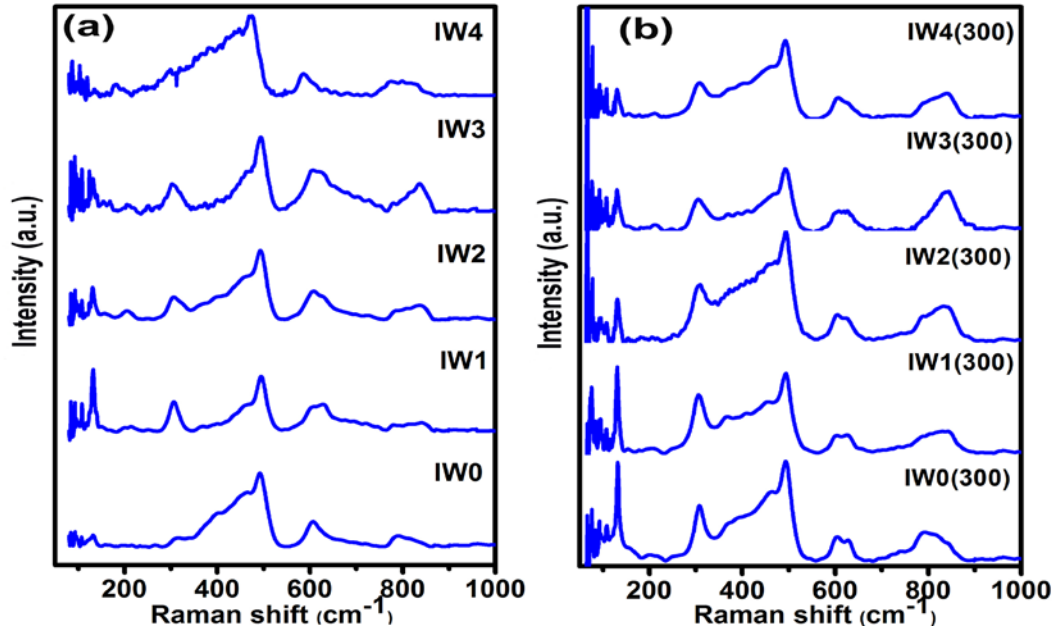


Fig. 4. Micro-Raman spectra of tungsten doped In_2O_3 films on quartz substrate by RF magnetron sputtering technique: (a) as-deposited (b) annealed at a temperature of 300 °C.

The band $\sim 132 \text{ cm}^{-1}$ in the undoped and doped films can be assigned to the vibration of In-O bond emerging from InO_6 structural unit [40]. This mode shows the highest intensity in IW1 film. The medium intense band $\sim 307 \text{ cm}^{-1}$ can be related to the $\delta(\text{InO}_6)$ bending vibration of InO_6 octahedra [42]. The weak band at 368 cm^{-1} can be assigned to the stretching vibrations of In-O-In which manifests the presence of oxygen vacancies in the structure [43]. The stretching vibrations $\nu(\text{InO}_6)$ of InO_6 octahedron results in the occurrence of bands ~ 495 and 628 cm^{-1} [42,43]. The bands ~ 604 and 830 cm^{-1} may have emerged from the quartz substrate [44,45]. All the expected vibrational modes of cubic bixbyite In_2O_3 structure is observed with moderate intensity in the Raman spectrum of IW1 film. Also, the vibrational modes obtained for the IW1 film are narrower compared to other tungsten doped films. This shows the better crystalline quality of the IW1 film compared to others.

The micro-Raman spectra of tungsten doped In_2O_3 films annealed at a temperature of $300\text{ }^\circ\text{C}$ are shown in Fig. 4(b). The spectra of all the films show sharper and more intense bands compared to that of the as-deposited films. This supports the improved crystalline nature of the annealed films.

Fig. 5 depicts the typical 2D AFM micrographs of as-deposited and annealed tungsten doped In_2O_3 films. The AFM images of all the films reveal a smooth, dense distribution of smaller grains. The IW1 film presents slightly bigger grains compared to others. The AFM image of IW4 film shows the distribution of grains of two different sizes. In the IW4(300) film, the grains are of almost same size. The root mean square (rms) surface roughness values calculated using WSxM 5.0 develop 6.4 software [46] is found to be in the range 1.25-2.98 nm for the as-deposited films and in the range 1.63-2.27 nm for the annealed films. AFM analysis reveal a smooth surface morphology for all the films which is beneficial for optoelectronic applications.

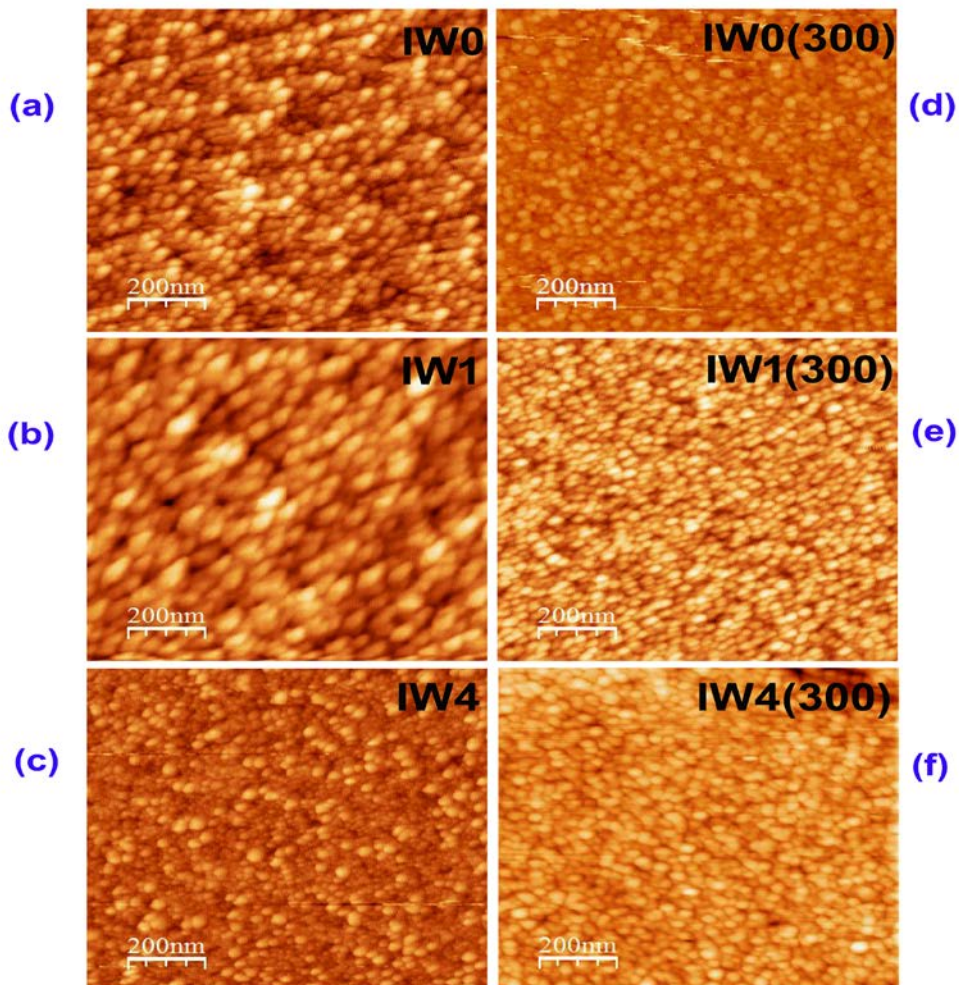


Fig. 5. 2D AFM images of typical tungsten doped In_2O_3 films: as-deposited films (a) IW0, (b) IW1 and (c) IW4 and annealed films (d) IW0(300), (e) IW1(300) and (f) IW4(300).

The chemical states of the elements in as-deposited tungsten doped In_2O_3 films are studied by XPS analysis. The acquired binding energies are calibrated using C 1s peak (284.8 eV) [47]. In 3d core level spectra of IW0, IW1 and IW4 films (Fig. 6(a), 6(b) and 6(c) respectively) exhibit the spin orbital splitting resulting in In $3d_{5/2}$ and In $3d_{3/2}$ peaks [48]. CASA XPS software is used to fit the peaks in the core level spectra. In $3d_{5/2}$ and In $3d_{3/2}$ peaks are observed at 444.38 and 451.97 eV respectively in the XPS spectrum of IW0 film. These peaks are observed at 444.51 and 452.08 eV respectively for the IW1 film and at 444.38 and 451.95 eV respectively for the IW4 film. The difference in binding energy of In $3d_{5/2}$ and In $3d_{3/2}$ in these films is found to be 7.57 eV which is in agreement with reported values [49,50]. A slight shift in In $3d_{5/2}$ and In $3d_{3/2}$ peaks to higher binding energy positions is observed for the IW1 film.

The O 1s core level spectra of IW0, IW1 and IW4 films are shown in Fig. 6(d), 6(e) and 6(f) respectively. For the films, deconvolution of the peak in the O 1s region yields two components- low binding energy component O(I) and high binding energy component O(II). Beena et al. obtained two components in the O 1s spectra ~529.49 eV and 531.05 eV for In_2O_3 films prepared at a substrate temperature of 300 K [51]. For undoped film, O(I) can be related to oxygen in the In_2O_3 lattice [52] and for tungsten doped films, O(I) can be related to oxygen in the In_2O_3 or WO_3 lattice [53,54]. O(II) can be correlated with oxygen in oxygen deficient regions [51,55]. For the undoped film IW0, the components are centred at 529.49 (O(I)) and 531.38 eV (O(II)). O(I) and O(II) peak positions of the IW1 film are at 530.02 and 531.68 eV respectively and for the film IW4, these peaks are at 529.73 and 531.51 eV respectively. The O 1s peaks in the tungsten doped films are observed at relatively higher binding energy positions compared to those in IW0 film. The intensity of O(I) and O(II) peaks and the area ratio ($O_{\text{II}}/O_{\text{I}}$) for the films IW0, IW1 and IW4 are given in Table II.

Table II Binding energy positions of In, O and W components, intensities of oxygen components and area ratio of high energy peak (O_{II}) to low energy peak (O_{I}) of O 1s from XPS data for typical as-deposited tungsten doped In_2O_3 films- IW0, IW1 and IW4.

Sample code	Binding energy positions (eV)						O(I) (%)	O(II) (%)	Area ratio $O_{\text{II}}/O_{\text{I}}$
	In $3d_{5/2}$	In $3d_{3/2}$	O(I)	O(II)	W $4f_{7/2}$	W $4f_{5/2}$			
IW0	444.38	451.97	529.49	531.38	-	-	22.57	77.43	3.43
IW1	444.51	452.08	530.02	531.68	35.32	37.27	47.46	52.54	1.11
IW4	444.38	451.95	529.73	531.51	35.10	37.13	32.90	67.10	2.03

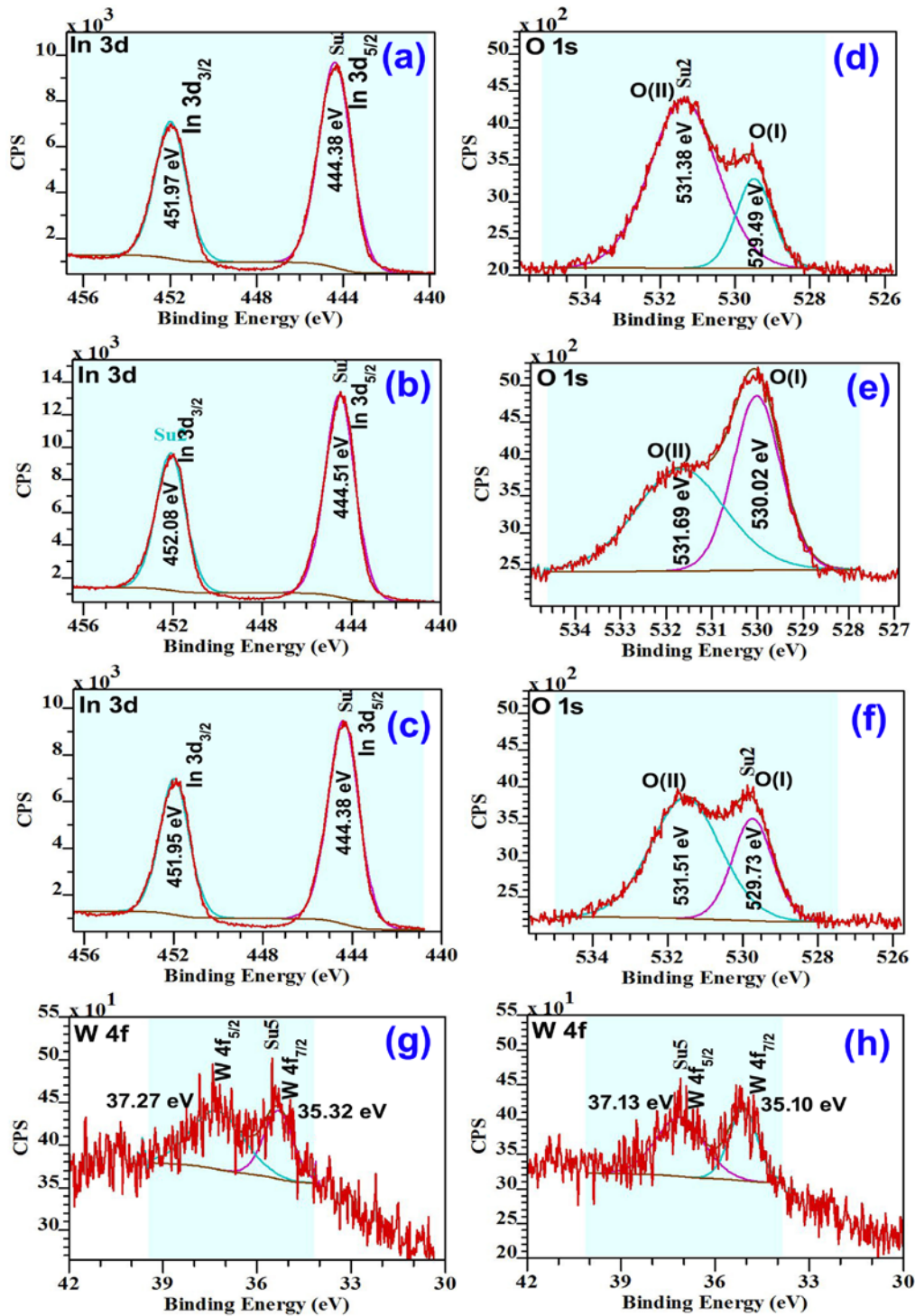


Fig. 6. In 3d core level spectra of typical as-deposited tungsten doped In_2O_3 films deposited by RF magnetron sputtering technique: (a) IW0, (b) IW1 and (c) IW4. O 1s core level spectra of typical as-deposited tungsten doped In_2O_3 films: (d) IW0, (e) IW1 and (f) IW4. W 4f XPS spectra of typical as-deposited tungsten doped In_2O_3 films: (g) IW1 and (h) IW4.

The values of intensities of O(I) and O(II) peaks show considerable variation with tungsten doping concentration. The value of intensity of the O(I) peak is highest for the IW1 film and the lowest for the IW0

film. The intensity of the O(II) peak is lowest for the IW1 film and highest for the IW0 film. The intensity variation of O(II) peak can be an indication of the variation of concentration of oxygen vacancies in the films.

For the films IW0, IW1 and IW4, the area ratio $\left[\frac{O(II)}{O(I)} \right]$ is found to be 3.43, 1.11 and 2.03 respectively.

The high value of the area ratio manifests the presence of large number of oxygen vacancies [56,57]. In the present case, this ratio is higher for the undoped film compared to the doped films IW1 and IW4. This implies

that the undoped film is highly oxygen deficient. Among the doped films, $\left[\frac{O(II)}{O(I)} \right]$ is the lowest for the

film IW1 and this indicates a reduction in the concentration of oxygen vacancies in this film. In indium zinc

oxide films, Kumar et al. [58] reported a decrease in the area ratio $\left[\frac{O(II)}{O(I)} \right]$ with increase in the atomic

ratio $[Zn/(Zn+In)]$. They attributed this decrease to the enhancement in film crystallinity with increase in atomic

ratio. For Zn doped In_2O_3 nanopyrramids, Bartolome et al. observed an increase in the lower binding energy

component of oxygen (O(I)) in regions with high Zn concentration and attributed this to the crystallinity

improvement with increasing Zn concentration [59]. The increase in the concentration of O(I) component and

the low value of area ratio observed for the IW1 film implies an improvement in crystallinity of this film which

is in accordance with the XRD analysis. An enhancement in the intensity of In 3d peaks is also observed for the

film IW1 compared to other doped films. The reduction in the O(I) component and the increase in the area ratio

for the film IW4 supports the declination in crystallinity at higher doping concentration.

Fig. 6(g) and 6(h) show the W 4f core level spectra of the typical tungsten doped In_2O_3 films-IW1 and IW4 respectively. By the deconvolution of W 4f peak, a doublet is obtained with binding energies of 35.32 and 37.27 eV for the IW1 film and at 35.10 and 37.13 eV for the IW4 film respectively. The higher binding energy component at 37.27 eV observed for the IW1 film and that at 37.13 eV for the IW4 film (Fig. 6(g) and 6(h)) can be ascribed to $W 4f_{5/2}$ level. The lower binding energy component at 35.32 eV for the film IW1 and that at 35.10 eV (Fig. 6(g) and 6(h)) for the IW4 film can be attributed to $W 4f_{7/2}$ level. These peaks indicate the presence of tungsten in 5+ oxidation state [60]. For the IW4 film, a slight shift in the positions of $W 4f_{5/2}$ and $W 4f_{7/2}$ peaks towards lower binding energy is observed compared with that of the IW1 film.

CONCLUSIONS

The present study focuses on the effect of tungsten doping and annealing at a temperature of 300 °C on the structural and morphological properties of In₂O₃ films synthesized at room temperature. XRD and Raman analysis reveals that both the as-deposited films and annealed films possess cubic bixbyite structure and exhibit strong preferred orientation along (222) plane. Tungsten doping and post-annealing of the films have profound effect on the crystallinity of In₂O₃ films. The deposition of films with smooth morphology is illustrated by AFM images. Incorporation of tungsten in the In₂O₃ lattice is supported by XPS analysis. XPS analysis reveals the presence of W⁵⁺ state in the tungsten doped films.

REFERENCES

- [1] W. Ahmed, *Nanomaterials and Nanotechnology*, (Manchester, United Kingdom: One Central Press (OCP) Ltd, 2016), pp.216.
- [2] V. Patil, S. Pawar, M. Chougule, P. Godse, R. Sakhare, S. Sen, P. Joshi, *J. Surf. Eng. Mater. Adv. Technol.* 1, 35 (2011).
- [3] S. S. Batros, G. S. Karam, *International journal of computational engineering research (IJCER)* 4(12) 15 (2014).
- [4] S. Hashmi, *Comprehensive Materials Processing*, (USA: Elsevier Inc.,2014), pp.77.
- [5] O. Kamoun, A. Boukhachem, C. Mrabet, A. Yumak, P. Petkova, K. Boubaker and M. Amlouk, *Bull. Mater. Sci.* 39(3), 777 (2016).
- [6] G. Korotcenkov, V. Brinzari and B. K. Cho, *International Journal of Electrical and Computer Engineering* 10(7) 884 (2016).
- [7] A. Murali, A. Barve, V. J. Leppert, and S. H. Risbud, *Nano Lett.* 1, 287 (2001).
- [8] K. Sreenivas, T. S. Rao, A. Mansingh and S. Chandra, *J. Appl. Phys.* 57, 384 (1985).
- [9] Z. Fang, H. Assaoudi, R. I. L. Guthrie, J. A. Kozinski and I. S. Butler, *J. Am. Ceram. Soc.* 90, 2367 (2007).
- [10] A. Tiwari, V.M. Bhosle, S. Ramachandran, N. Sudhakar, J. Narayan, S. Budak, A. Gupta, *Appl. Phys. Lett.* 88,142511 (2006).
- [11] Y.A.E. Aoud, M.C. Hickey, A.G. Kussow and A. Akyurtlu, *Phys. Status Solidi A*, 210 (12) 2644 (2013).
- [12] Ch. Y. Wang, Y. Dai, J. Pezoldt, B. Lu, Th. Kups, V. Cimalla and O. Ambacher, *Cryst. Growth Des.* 8(4), 1257 (2008).
- [13] S. Richter and A. Schwedt, *EMC 2008: Materials Science*, (Germany: Springer Science & Business Media,2008).
- [14] A. Walsh and C.R.A. Catlow, *J. Mater. Chem.* 20, 10438 (2010).
- [15] I. Hotovy, T. Kups, J. Hotovy, J. Liday, D. Buc, M. Caplovicova, V. Rehacek, H. Sitter, C. Simbrunner, A. Bonnani and L. Spiess, *Journal of electrical engineering* 61(6),382 (2010).
- [16] A.E.Fakir, M. Sekkati, G. Schmerber, A. Belayachi, Z. Edfouf, M. Regragui, F.C.El Moursli, Z. Sekkat, A. Dinia, A. Slaoui and M. Abd-Lefdil, *Phys. Status Solidi C*, 14(10), 1700169 (2017).
- [17] X. Li, Q. Zhang, W. Miao, L. Huang and Z. Zhang, *Thin Solid Films* 515, 2471 (2006).
- [18] Y. Abe and N. Ishiyama, *Mater. Lett.* 61, 566 (2007).
- [19] D.R. Acosta and A.I. Martínez, *Thin Solid Films* 515, 8432 (2007).
- [20] J. Pan, W. Wang, D. Wu, Q. Fu and D. Ma, *J. Mater. Sci. Technol.* 30, 644 (2014).
- [21] Y. Li, W. Wang, J. Zhang and R. Wang, *Rare Met.* 31, 158 (2012).
- [22] I.G. Samatov, B.R. Jeppesen, A.N. Larsen and S.K. Ram, *Appl. Phys. A.* 122, 458 (2016).
- [23] E. Parsianpour, D.Raoufi, M. Roostaei, B.Sohrabi and F. Samavat, *Adv. Mater. Phys. Chem.* 7, 42 (2017).
- [24] L.T. Yan, R.E.I. Schropp, *Thin Solid Films* 520, 2096 (2012).
- [25] Z. Lu, F. Meng, Y. Cui, J. Shi, Z. Feng and Z. Liu, *J. Phys. D. Appl. Phys.* 46, 75103 (2013).

- [26] S. Muranaka, Y. Bando and T. Takada, *Thin Solid Films* 151, 355 (1987).
- [27] P. K. Song, Y. Shigesato, M. Kamei and I. Yasui, *Jpn. J. Appl. Phys.* 38, 2921 (1999).
- [28] J.-O. Park, J.-H. Lee, J.-J. Kim, S.-H. Cho and Y.K. Cho, *Thin Solid Films*. 474, 127 (2005).
- [29] B.D. Cullity, *Elements of X-Ray Diffraction*, (Massachusetts: Addison-Wesley Publishing Company, Inc., 1956).
- [30] Kafizas and I.P. Parkin, *J. Am. Chem. Soc.* 133, 20458 (2011).
- [31] M.R. Pai, J. Majeed, A.M. Banerjee, A. Arya, S. Bhattacharya, R. Rao and S.R. Bharadwaj, *J. Phys. Chem. C* 116, 1458 (2012).
- [32] V. Sharma, A. McDannald, M. Staruch, R. Ramprasad and M. Jain, *Appl. Phys. Lett.* 107, 012901 (2015).
- [33] Y. Meng, X. Yang, H. Chen, J. Shen, Y. Jiang, Z. Zhang and Z. Hua, *Thin Solid Films*. 394, 219 (2001).
- [34] R.K. Shukla, A. Srivastava, A. Srivastava and K.C. Dubey, *J. Cryst. Growth*. 294(2), 427 (2006).
- [35] H. Kim, J.S. Horwitz, S.B. Qadri and D.B. Chrisey, *Thin Solid Films*. 420–421, 107 (2002).
- [36] H. Kim, A. Piqué, J.S. Horwitz, H. Murata, Z.H. Kafafi, C.M. Gilmore and D.B. Chrisey, *Thin Solid Films*. 377–378, 798 (2000).
- [37] R. Eason, *Pulsed Laser Deposition of Thin Films*, (New Jersey, United States of America: John-Wiley and Sons, Inc., 2007), pp.682.
- [38] A.L. Patterson, *Physical Review* 56, 978 (1939).
- [39] G.K. Williamson and W.H. Hall, *Acta Metall.* 1(1), 22 (1953).
- [40] J. Gan, X. Lu, J. Wu, S. Xie, T. Zhai, M. Yu, Z. Zhang, Y. Mao, S.C.I. Wang, Y. Shen and Y. Tong, *Sci. Rep.* 3, 1021 (2013).
- [41] L. Guo, X. Shen, G. Zhu and K. Chen, *Sensors Actuators B. Chem.* 155, 752 (2011).
- [42] S. Elouali, L.G. Bloor, R. Binions, I.P. Parkin, C.J. Carmalt and J.A. Darr, *Langmuir* 28, 1879 (2012).
- [43] G.M. Kumar, A.M. Kumar, P. Ilanchezhian and T.W. Kang, *Nanoscale*. 6, 11226 (2014).
- [44] J.W. Chan, T. Huser, S. Risbud and D.M. Krol, *Opt. Lett.* 26(21), 1726 (2001).
- [45] R.S. Krishnan, *Nature* 155, 452 (1945).
- [46] I. Horcas, R. Fernández, J.M.G.-Rodríguez, J. Colchero, J. G.-Herrero and A.M. Baro, *Rev. Sci. Instrum.* 78, 013705 (2007).
- [47] P. Babelon, A.S. Dequiedt, H. Mostefa-Sba, S. Bourgeois, P. Sibillot and M. Sacilotti, *Thin Solid Films* 322, 63 (1998).
- [48] S. Hu, B. Chi, J. Pu and L. Jian, *J. Mater. Chem. A*. 2, 19260 (2014).
- [49] B. Ballarin, M.C. Cassani, C. Maccato and A. Gasparotto, *Nanotechnology* 22, 275711 (2011).
- [50] W.J. Kim, D. Pradhan and Y. Sohn, *J. Mater. Chem. A*. 1, 10193 (2013).
- [51] D. Beena, K.J. Lethy, R. Vinodkumar, V.P.M. Pillai, V. Ganesan, D.M. Phase and S.K. Sudheer, *Appl. Surf. Sci.* 255, 8334 (2009).
- [52] Y. An, S. Wang, L. Duan, J. Liu and Z. Wu, *Appl. Phys. Lett.* 102, 212411 (2013).
- [53] X.G. Wang, Y.S. Jang, N.H. Yang, L. Yuan and S.J. Pang, *Surf. Coatings Technol.* 99, 82 (1998).
- [54] P. Chatchai, Y. Murakami, S. Kishioka, A.Y. Nosaka and Y. Nosaka, *Acta*. 54, 1147 (2009).
- [55] J.C.C. Fan and J.B. Goodenough, *J. Appl. Phys.* 48, 3524 (1977).
- [56] S.-H. Kim, H.-S. Choi and K.-D. Jung, *Cryst. Growth Des.* 16(3), 1387 (2016).
- [57] D.V. Shinde, D.Y. Ahn, V.V. Jadhav, D.Y. Lee, N.K. Shrestha, J. K. Lee, H.Y. Lee, R. S. Mane and S.-H. Han, *J. Mater. Chem. A*. 2, 5490 (2014).
- [58] B. Kumar, H. Gong and R. Akkipeddi, *J. Appl. Phys.* 97(6), 063706 (2005).
- [59] J. Bartolomé, D. Maestre, M. Amati, A. Cremades and J. Piqueras, *J. Phys. Chem. C*. 115(6), 8354 (2011).
- [60] Z. Si, D. Weng, X. Wu, Y. Jiang and B. Wang, *Catal. Sci. Technol.* 1, 453 (2011).